AIP Advances

Reversible conductance switching characteristics in a polymer-In_2O_3 nanocrystals junction

Cite as: AIP Advances 4, 067127 (2014); https://doi.org/10.1063/1.4884303
Submitted: 01 December 2013 • Accepted: 06 June 2014 • Published Online: 16 June 2014

Jongmin Kim, Dong Uk Lee, Yongcheol Jo, et al.

ARTICLES YOU MAY BE INTERESTED IN

Waltzing of a helium pair in tungsten: Migration barrier and trajectory revealed from first-principles
AIP Advances 4, 067128 (2014); https://doi.org/10.1063/1.4884304

Residue-free fabrication of high-performance graphene devices by patterned PMMA stencil mask
AIP Advances 4, 067129 (2014); https://doi.org/10.1063/1.4884305

Nitrobenzene anti-parallel dimer formation in non-polar solvents
AIP Advances 4, 067130 (2014); https://doi.org/10.1063/1.4884393

AIP Advances Biophysics & Bioengineering Collection Read Now!

AIP Publishing

© 2014 Author(s).

AIP ADVANCES **4**, 067127 (2014)

Reversible conductance switching characteristics in a polymer-In_2O_3 nanocrystals junction

Jongmin Kim,[1] Dong Uk Lee,[2] Yongcheol Jo,[1] J. Han,[1] H. S. Kim,[1] A. I. Inamdar,[1] W. Jung,[1] Hyunsik Im,[1,a] and Eun Kyu Kim[2,b]
[1]*Division of Physics and Semiconductor Science, Dongguk University, Seoul 100-715, Korea*
[2]*Department of Physics, Hanyang University, Seoul 133-791, Korea*

(Received 1 December 2013; accepted 6 June 2014; published online 16 June 2014)

A transparent polymer-based resistive switching device containing In_2O_3 nanocrystals (NCs) is fabricated, and its nonvolatile memory characteristics are evaluated. Very clear reversible counter-clockwise bipolar-type resistive switching phenomena are observed. Stable retention is demonstrated. An Analysis of the temperature dependence of the bistable resistance states reveals additional features, not reported in previous studies, that the observed resistance switching is due to oxygen ions drift-induced redox reactions at the polymer/In_2O_3 NCs interface. The RESET and SET switching times (τ_{RESET} and τ_{SET}), which are defined as pulse widths extrapolated by the steepest slopes in the transition region, are $\tau_{RESET} \sim 550$ nsec and $\tau_{SET} \sim 900$ nsec. The authors propose that microscopic potential modification occurring near the polymer/In_2O_3 NCs boundaries plays a key role in determining resistive switching properties. © *2014 Author(s). All article content, except where otherwise noted, is licensed under a Creative Commons Attribution 3.0 Unported License.* [http://dx.doi.org/10.1063/1.4884303]

Electrically induced resistive switching phenomena between two different resistance states, a high resistance state (HRS) and a low resistance state (LRS), is often observed in various metal-I-metal structures, in which the "I" layer ranges from the insulating metal oxides,[1–4] to more complex materials,[5–11] such as organic matter.[12,13] Besides their intriguing physics, this phenomenon has attracted considerable attention in the memory industry due to its potential application in next-generation nonvolatile memories, which are often abbreviated as ReRAM or RRAM.[14–17] Despite intensive research efforts, the unique combination of resistive switching material and device configuration that can play a leading role in the ReRAM development has not yet been found. Thus, research effort has been made in two directions. One is to improve and optimize the resistive switching properties in already-known resistive switching materials and device structures; the other is to find novel resistive switching materials and device configurations.

It has been demonstrated that hybrid inorganic/organic nano-composites show nonvolatile resistive switching.[18–20] Due to the diversity of organic films that are used, and their good process compatibility, miniaturized dimensions, and possibility for molecular design through various chemical synthesis techniques, these hybrid-type resistive switching devices are regarded as one of the promising candidates for new functional non-volatile memory applications. In this work, we demonstrate that bipolar resistive switching non-volatile memory characteristics can be obtained using an In_2O_3 nanocrystals (NCs) embedded polyimide (PI)/ZnO heterojunction structure grown on a transparent substrate.[21–25] Based on analyses of current-voltage (*I-V*) characteristics in different resistive states and the temperature dependence of the bi-stable resistance states, which reveal additional features on switching transport, we propose a resistive switching mechanism.

[a]Electronic mail: hyunsik7@dongguk.edu
[b]Electronic mail: ek-kim@hanyang.ac.kr

 © Author(s) 2014

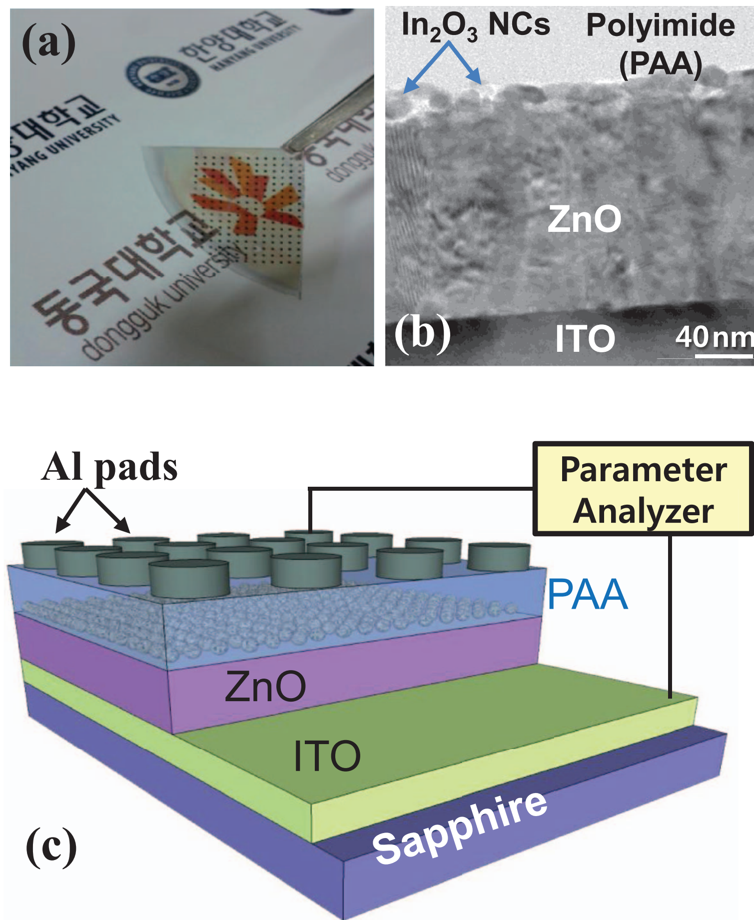

FIG. 1. (a) Photograph of transparent ReRAM devices. The regularly positioned dots are Al top electrodes. (b) Cross-sectional transmission electron microscope (TEM) image of the memory device with In_2O_3 nanocrystals (NCs). (c) Three-dimensional schematic of ReRAM devices with In_2O_3 NCs at the polyimide (PI)/ZnO interface.

In_2O_3 nanocrystal memory devices embedded in polyimide layers were fabricated on double-side polishing sapphire wafers. An indium-tin-oxide (ITO) layer with a thickness of 190 nm was grown by radio-frequency (RF) magnetron sputter. Subsequently, a ZnO layer with a thickness of 140 nm was deposited on the ITO layer, by RF magnetron sputtering of a ZnO target. These two sputtering processes were carried out at room temperature under the same conditions, of working power: 60 W and working pressure: 6×10^{-3} Torr. The indium with a thickness of 5 nm was deposited onto a ZnO/ITO/sapphire substrate, using a thermal evaporator. Then, 50 nm-thick polyamic acid (PAA) was spin-coated onto the deposited indium film. Here, a commercial biphenyl-tertracarboxylic dianhydride-phenylen diamine (BPDA-PDA) type PAA was used. The PAA solution was composed of BPDA-PDA in N-methyl-2-pyrrolidone (3 wt%). After the indium dissolving process for 24 hours in vacuum desiccators, the sample was cured at 135 °C for 30 min and at 400 °C for 1 hour, in an N_2 atmosphere. In_2O_3 NCs formed inside the polyimide (PI) matrix during the curing process, by a chemical reaction with indium ions and oxygen attached to the PAA. For electrical measurements, 200 μm-wide Al top electrodes were deposited by thermal evaporator, using a shadow mask. We applied a bias voltage to the top Al electrode, with the bottom ITO electrode grounded. The fabricated device and its cross-sectional transmission electron microscope (TEM) image are shown in Figure 1. In the absence of the ZnO layer, the observed resistive switching phenomenon is unstable with a poor reliability. Thus, regardless of its complex structure, we intentionally included the ZnO layer between In_2O_3 NCs and the ITO.

Figure 2(a) shows the measured resistive switching *I-V* curves for the device under consecutive voltage-bias sweeping operations. The black solid curves represent one measured cycle of resistive

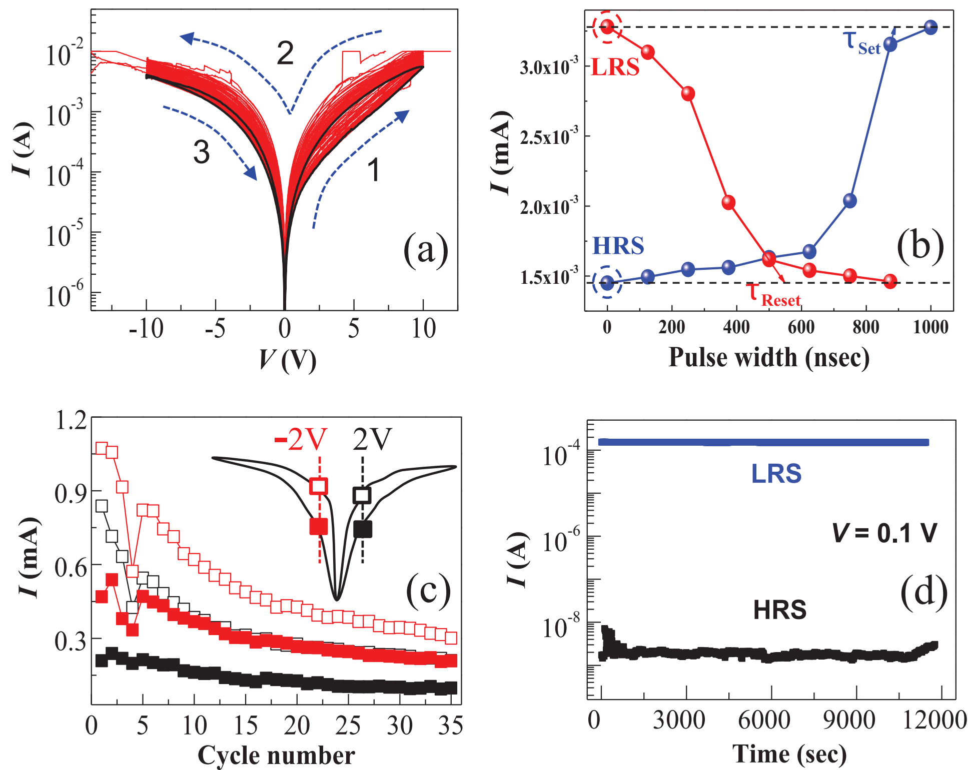

FIG. 2. (a) Non-volatile bipolar resistive switching *I-V* characteristics. The numbers represent the counter-clockwise (CCR) switching direction. (b) The variation of the output current at 0.1 V as a function of pulse-voltage width after voltage pulse operations. The dash lines correspond to the original current level before each pulse operation. (c) Endurance performance at ±2 V. The open and closed squares represent the low and high resistance states, respectively. (d) Retention performance at 0.1 V.

switching. The device shows bipolar resistive switching behaviors with a counter-clockwise switching mode (1 → 2 → 3 → 1), as indicated by the dotted blue arrows. Thus, the high resistance state (HRS) switches into the low resistance state (LRS) in the forward bias polarity (SET or Writing process), and its opposite switching (LRS → HRS) occurs in the reverse bias polarity (RESET or Erasing process). It should be noted that although the resistive switching performance (or quality) differs sample by sample (even pad by pad on the same wafer), the switching characteristics are bipolar-type, with a counter-clockwise switching mode. It would be reasonable to presume that the observed different switching performance for different samples (or pads on the same wafer) is related to the non-uniformity of the In_2O_3 NCs embedded in the PI layer beneath the Al pads, rather than the alteration of transport mechanisms. We also note that the resistive switching features in our samples do not require an electroforming process. The on/off ratio in the low voltage region below ±0.5 V varies at each switching cycle between $\sim 10^1$ and $\sim 10^5$.

In order to confirm the importance of the embedded In_2O_3 NCs in the observed resistive switching phenomena, we also performed similar resistive switching current-voltage (*I-V*) measurements in devices without In_2O_3 NCs in the PI layer. We confirmed that PI/ZnO structures without the In_2O_3 NCs do not show the resistive switching behaviour, indicating that the In_2O_3 NCs play a key role in determining the observed resistive switching phenomena. Charging effect in the device may contribute to the observed resistive switching transport, but its measured capacitance voltage characteristics suggest that the charging effect in the device is not significant enough to produce the observed voltage bias polarity dependent hysteresis.

The switching times are estimated by measuring dc *I-V* curves after applying pulse voltage-bias inputs of ±10 **V** with different widths from 125 to 1000 nsec.[5] Figure 2(b) shows the measured output current at +0.1 V after each pulse voltage operation as a function of voltage-pulse width

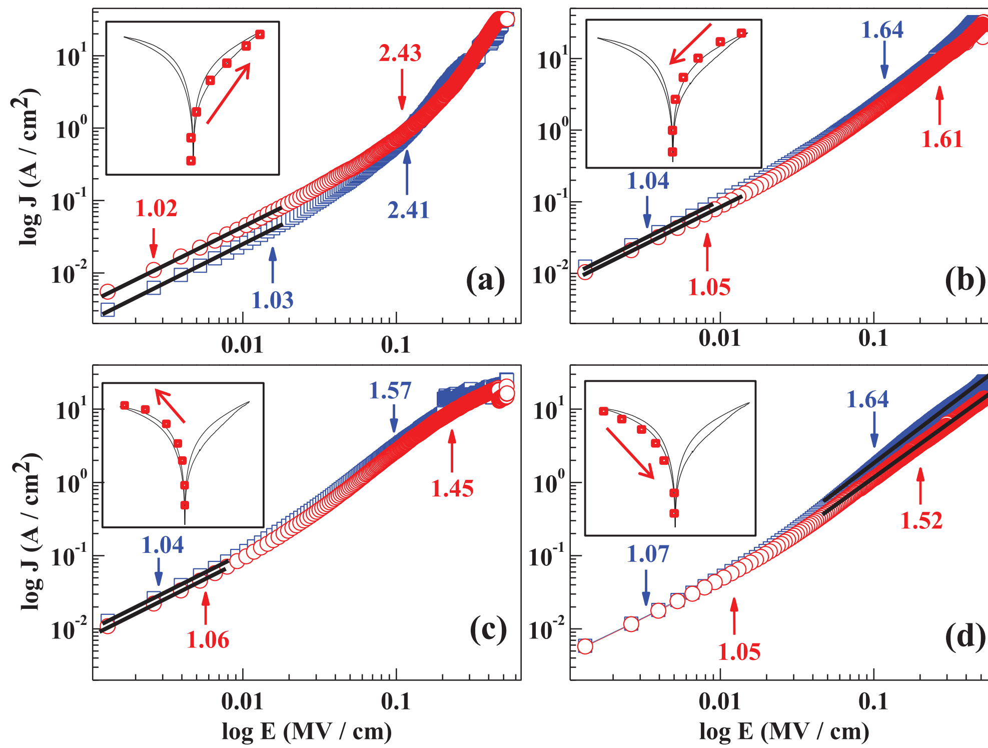

FIG. 3. The log *J*- log *E* plots for the high resistance state and the low resistance state for voltage sweeping. (a) at the forward-bias HRS, (b) during the set process with a positive voltage, (c) at the reverse-bias LRS, (d) during the reset process with a negative voltage. The blue and red lines represent the 7th and 15th resistive switching *I-V* curves, respectively.

for the HRS → LRS and HRS → LRS transitions. The dash lines represent the original current level before the pulse operation. As the pulse width is increased, the current levels of the HRS and the LRS approach the current levels of the LRS and the HRS respectively. Here, the RESET (LRS → HRS) and SET (HRS → LRS) switching times, τ_{RESET} and τ_{SET}, are defined as pulse widths extrapolated by the steepest slopes in the transition region. $\tau_{RESET} \sim 550$ nsec and $\tau_{SET} \sim 900$ nsec.

Figure 2(c) shows the endurance test (HRS and LRS currents at ±2 V as a function of switching cycle). As the switching cycle increases, the HRS and LRS currents in both bias polarities tend to slowly decrease, and become stabilized. The currents in the negative voltage region are larger than those in the positive voltage region. This is related to the asymmetric device structure. The switching cycle induced fatigue of the device is not excellent, compared with that of previously reported binary oxide based ReRAM devices.[14–17] We presume that this is because the PI layer is degraded by the repeated application of high electric fields.

Another important non-volatile memory characteristic of the device is its retention properties. Figure 2(d) shows the time-dependent current evolution of the LRS and the HRS at an operating voltage of 0.1 V. The retention properties in both resistance states are very stable, confirming the non-volatile memory behavior of the device. Note that the fluctuating current in the HRS is presumably because the current level of the HRS is too low.

In order to figure out the electrical nature of the conducting channel in each resistance state, we plot the current density (J) as a function of electric field (E) in the logarithmic scale, and their slopes are fitted, as shown in Fig. 3. The current density J in each resistance state increases linearly with a slope of ∼1, until the electrical field reaches 0.1 MV/cm. It should be noted that the measured values of the slopes (Δ) and general *J-E* features in the log-log plots are consistent, regardless of the switching cycle. Δ ∼1 in the low electric field regime for all the resistance states means that the low-field transport in each resistance state is governed by a similar ohmic conduction mechanism.[26] However, as the field increases further, Δ becomes larger. A noticeable interesting feature in the

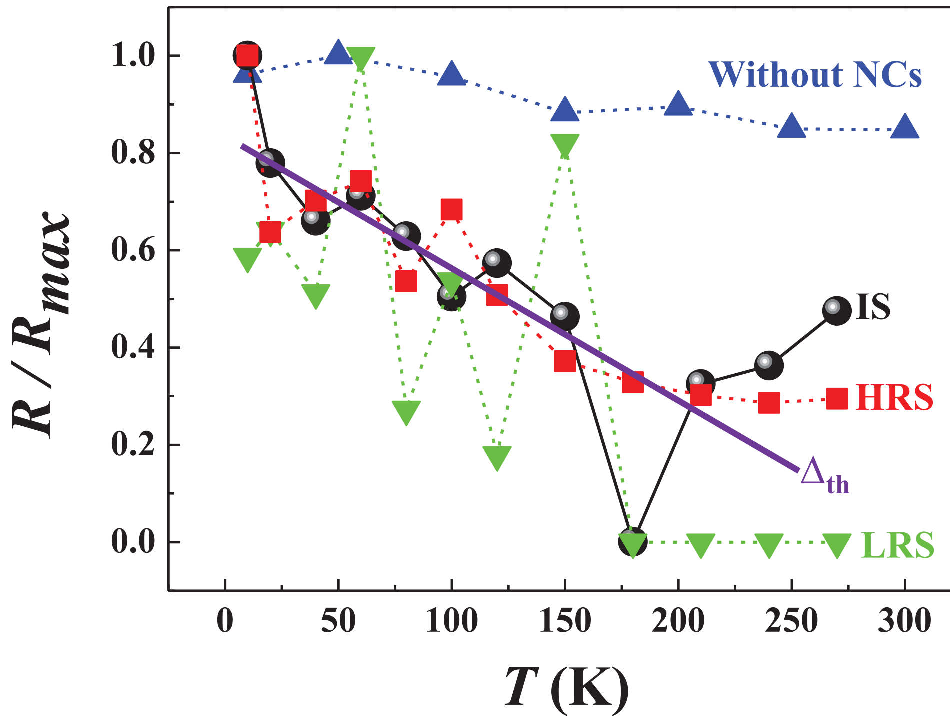

FIG. 4. Temperature dependent normalized resistance of the initial resistance state (IS), low resistance state (LRS) and high resistance state (HRS) of the PI-In_2O_3/ZnO device, and the PI/ZnO device without nanocrystals. All resistance values are measured at 0.1 V.

high field data is that Δ of ∼2.4 in the HRS of the SET process (Fig. 3(a)) is much larger than the Δ of ∼1.55 ± 0.1 observed in other resistance states (Figs. 3(b)–3(d)). The dramatically increased Δ value in the high field regime of the LRS implies that a different transport mechanism occurs making the device more electrically conductive. The physical origin of the dramatically enhanced conductivity can be due to the electrically induced oxygen ion movement nearby the PI/In_2O_3 NCs interface. Recently, oxygen ion drift-induced complementary resistive switching was observed in Ti-oxide based homo- and hetero-junction systems.[27] It is found that the field dependence of the current density in the PI/ZnO device is comparable with those in the HRS and the LRS in the low field regime (data not shown), implying that the basic electrical transport in both devices is described by the same mechanism.

Analysis on the temperature dependence of the bistable resistance states also provides valuable information on the transport mechanism in each resistance state.[28,29] If the conducting channel has a metallic characteristic, its resistance would decrease in a similar way to that of electrical conduction in metals. Such metallic conducting channels, called conducting filaments, have been identified in various binary metal oxide systems where unipolar-type resistive switching is observed.[30–33] However, if a modification in the potential configuration at the heterojunction interface plays a key role in determining the observed resistive switching phenomena, temperature dependences of the LRS and the HRS are expected to show a similar transport to that observed in metal-insulator-metal structures. Figure 4 shows the measured temperature (T) dependences of the normalized resistance (R/R_{max}) in different resistance states. The resistance (R) values were taken in the ohmic-like low voltage region below 0.1 V. As T decreases in the range between 60 K and 270 K, R in the LRS, the HRS and the IS increases in a similar way to electrical conduction in a metal/insulator/metal structure, where the insulator acts as a potential barrier, showing thermal activation. However for the LRS, its resistance value fluctuates with decreasing temperature. For the HRS and the IS, assuming $R_{60K}/R_{270K} \propto \exp(-\Delta_{th}/k_BT)$, where Δ_{th} represents the *effective* potential barrier height, Δ_{th} is estimated to be 6.8 meV. This analysis on the temperature dependent conduction in each resistance state suggests that the observed reversible resistance switching is not explained by the repeatable

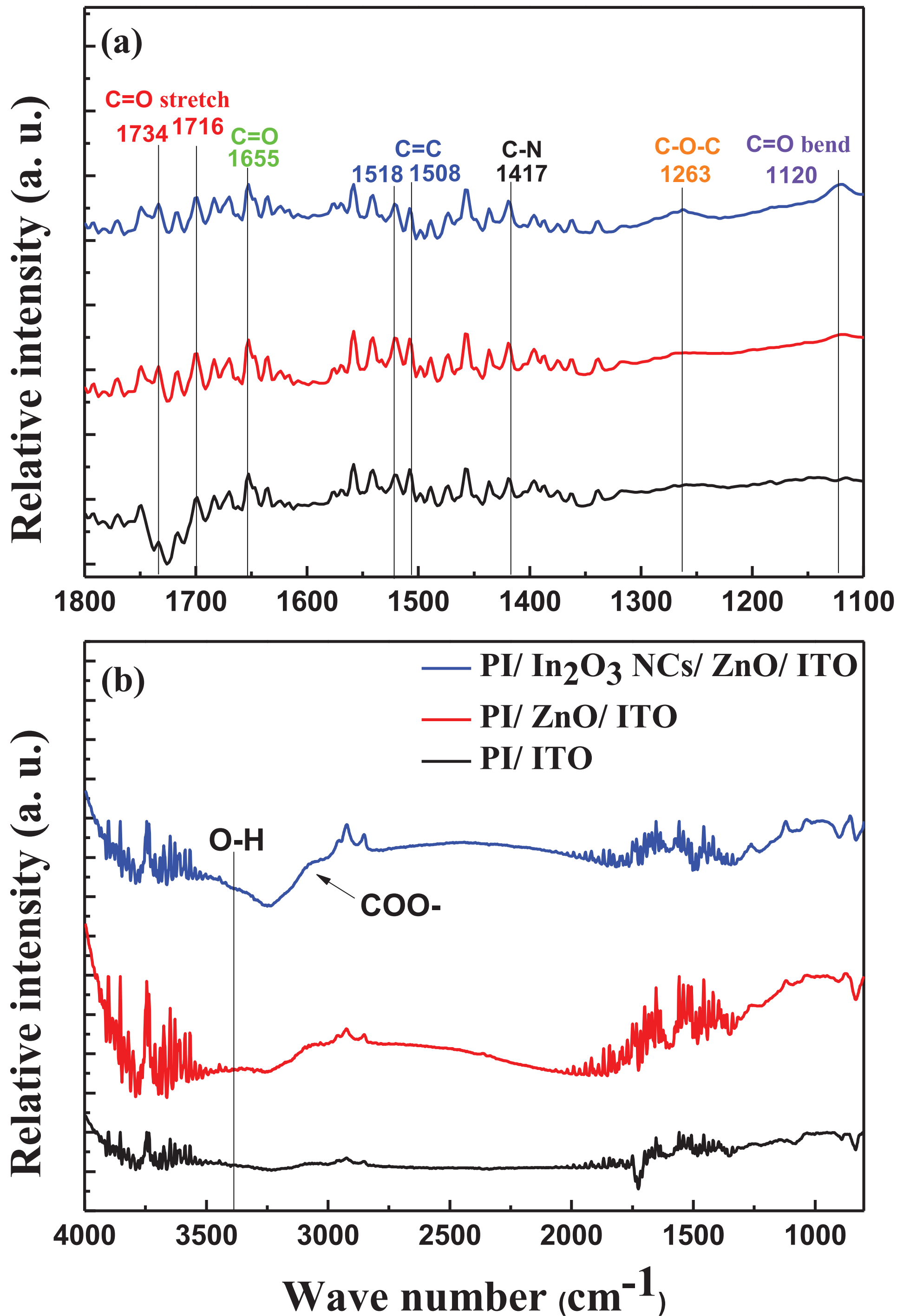

FIG. 5. Fourier transform infrared spectroscopy spectra of the PI layer for different wave number regions. (a) 1100 $\sim$ 1800 cm^{-1} and (b) 800 $\sim$ 4000 cm^{-1}.

formation and rupture of metallic filaments across the PI layer. For the PI/ZnO device, its temperature dependence is relatively very small compared with those in the HRS and the IS of the PI-In_2O_3/ZnO device. This is presumably because the In_2O_3 NCs in the device act as additional effective potential barrier and this is basically consistent with our switching model.

The chemical structure variation of the PI in the device is investigated by using Fourier transform infrared spectroscopy (FTIR) (see Figure 5). Well-defined C=O stretch, O-H stretching bonds,

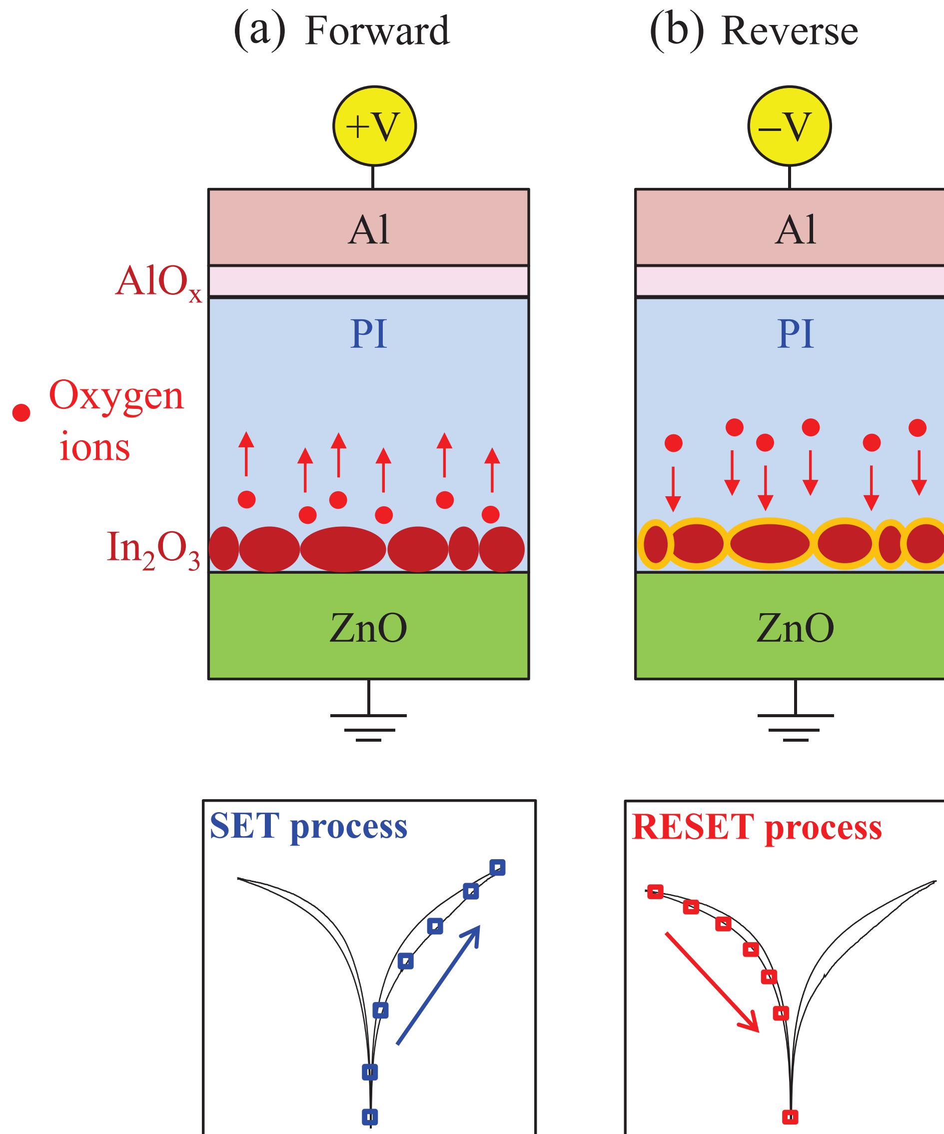

FIG. 6. Schematic of bipolar resistive switching model. (a) Oxygen ions are pulled toward the top Al electrode under the forward bias voltage. In the SET process where the oxygen ions move away from the NCs, the boundaries of the In_2O_3 NCs become transparent electrically. (b) In the reverse bias polarity (RESET process) where the oxygen ions are pushed back towards In_2O_3 NCs boundaries. The In_2O_3 NCs becomes opaque electrically acting as a resistive barrier.

C-O-C & C=O bands and carboxylate ion COO- features appear in the FTIR spectra. It is obvious that presence of the In_2O_3 NCs affects the chemical structure variation of the PI layer, presumably due to the chemical reaction between the indium thin film and the PAA layer during the curing process.

In order to exclusively elucidate the importance of the NCs on the observed resistive switching phenomena, we conducted a comparative experiment using devices with and without In_2O_3 NCs. Resistive switching occurred only in the sample with In_2O_3 NCs. This strongly supports that the NCs play a dominant role in the observed switching phenomena.

The schematic switching model of the Al/In_2O_3 NCs embedded PI/ZnO/ITO device is illustrated in Fig. 6. In the initial high resistance state (IS), because the PI layer is much resistive compared with other layers (In_2O_3 and ZnO), the bias voltage is mostly applied across the PI layer, and the electrical transport is governed by microscopic conduction paths across the PI layer. A very thin

naturally-formed AlO_x interfacial layer exists between the Al top electrode and the PI layer. When a high forward bias voltage is applied, negatively-charged oxygen ions are created, leaving oxygen vacancies in the In_2O_3 NCs, and move away from the PI/In_2O_3 NCs boundaries (Fig. 6(a)). Because this process makes the PI/In_2O_3 NCs interface more conductive, when the voltage is swept back its original resistance value deceases. This process corresponds to switching from the HRS to the LRS (SET process). When a negative bias voltage is applied to the top Al pad, negatively charged oxygen ions move back towards the NCs, forming relatively high-resistive PI/In_2O_3 NCs boundaries (Fig. 6(b)). This leads to switching from the LRS to the HRS (RESET process). Thus, the observed resistive switching behavior is due to the redox chemical reaction, which changes the Schottky barrier height and width at the PI/NCs interface. The observed shorter τ_{RESET} for the LRS → HRS transition implies that the chemical redox reaction (described in Fig. 6(b)) near the PI/In_2O_3 NCs boundaries is faster than its opposite process (described in Fig. 6(a)).

In the IS, the asymmetric transport is determined mainly by the potential barrier profiles at the junction interfaces. The potential barrier height and shape at each interface are given differently, depending on the atomic nature of the constituting materials.[34] This asymmetric potential profile explains the observed asymmetric *I-V* characteristics in the IS. During the RESET process (LRS → HRS), because In is the more chemically active metal compared to Al, the redox electrochemical reaction may occur favorably at the In_2O_3-PI interface, modifying the electrical conductivity at the interface. In the SET process (HRS → LRS) under the opposite bias-voltage polarity where reverse electrochemical reaction process occurs, the high resistive state at the interface is restored.

The observed counter clockwise resistive-switching (CCR) mode may be determined by the material properties of constituting elements, and device structure of the ReRAM. One of the dominant parameters determining the CCR mode is the electronegativity near the top AlO_x/PI and bottom In_2O_3/PI interfaces. Because ZnO is a very stable material having a large oxygen binding energy, ∼530 eV,[35,36] redox electrochemical reactions at the In/ZnO and In_2O_3 NCs/ZnO interfaces are unlikely. This is confirmed by the sharp ZnO/InO_x interface, without any signature of In-Zn-O alloys, in the TEM image (Figure 1). This redox reaction at the PI/In_2O_3 NCs interface explains the observed counter-clockwise switching mode.

In summary, we demonstrated non-volatile bipolar-type resistive switching in an In_2O_3 NCs embedded polyimide (PI)/ZnO heterojunction device. Its non-volatile memory characteristics were confirmed by performing endurance and retention measurements. The observed on/off ratio was as large as 10^5. The RESET (LRS → HRS) and SET (HRS → LRS) switching times are found to be ∼550 nsec and $\tau_{SET} \sim 900$ nsec, respectively. The analyses of the current-voltage characteristics and temperature-dependent conduction in each resistance state suggest that the origin of the bipolar-type resistive switching involves the redox electrochemical reactions at the PI/In_2O_3 NCs interface, and this is caused by the drift of oxygen ions that are locally distributed nearby the polyimide (PI) and In_2O_3 NCs boundaries.

This work was partially supported by the National Research Foundation (NRF) of Korea grant funded by the ministry of Education (Grant Nos. 2012R1A1A2008517 and 2013-044975). EKK acknowledges to the Mid-career researcher program through the NRF grant (NRF-2013-1015824).

[1] Y. H. Do, J. S. Kwak, Y. C. Bae, J. H. Lee, Y. Kim, H. Im, J. P. Hong, Curr. Appl. Phys. **10**, e71 (2010).
[2] X.-J. Zhu, J. Shang, and R.-W. Li, Front. Mater. Sci. (2012).
[3] R. Waser and M. Aono, Nature Mater. **6**, 833 (2007).
[4] K. Jung, Y. Kim, W. Jung, H. Im, B. Park, J. Hong, J. Lee, J. Park, and J.-K Lee, Appl. Phys. Lett. **97**, 233509 (2010).
[5] M. K. Yang, K. Jung, Y. Kim, T. K. Ko, H. Im, J.-W. Park, and J.-K. Lee, Jpn. J. Appl. Phys. **49**, 111101 (2010).
[6] K. Jung, Y. Kim, Y. S. Park, W. Jung, J. Choi, B. Park, H. Kim, W. Kim, J. Hong, and H. Im, J. Appl. Phys. **109**, 054511 (2011).
[7] A. I. Inamdar, Y. S. Kim, B. U. Jang, H. Im, W. Jung, D.-Y. Kim, H. Kim, Thin Solid Films **520**, 5367 (2012).
[8] A. I. Inamdar, J. Kim, B. Jang, D. Kim, H. Im. W. Jung, and H. Kim, Jpn. J. Appl. Phys. **51**, 104102 (2012).
[9] C. Yoshida, K. Tsunoda, H. Noshiro, and Y. Sugiyama, Appl. Phys. Lett. **91**, 223510 (2007).
[10] Y. H. Do, J. S. Kwak, Y. C. Bae, K. Jung, H. Im, J. P. Hong, Thin Solid Films **518**, 4408 (2010).
[11] B. U. Jang, A. I. Inamdar, J. Kim, W. Jung, H. Im, H. Kim, J. P. Hong, Thin Solid Films **520**, 5451 (2012).
[12] A. Ruchi, P. Kumar, and S. Ghosh, IEEE Trans. Electron Dev. **55**, 2795 (2008).
[13] A. Bandyopadhyay and A. J. Pal, Appl. Phys. Lett. **82**, 1215 (2003).
[14] H. Akinaga and H. Shima, Proceedings of the IEEE **98**, 12 (2010).
[15] A. Sawa, Materials today **11**, 6 (2008).

[16] J. J. Yang, M. D. Pickett, X. Li, D. A. A. Ohlberg, D. R. Stewart, and R. S. Williams, Nature Nanotechnol. **3**, 429 (2008).
[17] K. Kinoshita, T. Tamura, M. Aoki, Y. Sugiyama, and H. Tanaka, Appl. Phys. Lett. **89**, 103509 (2006).
[18] D. Panda, C.-Y. Huang, and T.-Y. Tseng, Appl. Phys. Lett. **100**, 112901 (2012).
[19] D. Panda, T.-Y. Tseng, Thin Solid Films **531**, 1 (2013).
[20] J. H. Jung, J. H. Kim, T. W. Kim, M. S. Song, Y. H. Kim, S. Jin, Appl. Phys. Lett. **89**, 122110 (2006).
[21] Q. Liu, S. Long, H. Lv, W. Wang, J. Niu, Z. Huo, J. Chen, and M. Liu, ACS Nano **4**, 6162 (2010).
[22] Q. Liu, S. Long, W. Wang, S. Tanachutiwat, Y. Li, Q. Wang, M. Zhang, Z. Huo, J. Chen, and M. Liu, IEEE Electron Device Lett. **31**, 1299 (2010).
[23] L. Chen, H.-Y. Gou, Q.-Q. Sun, P. Zhou, H.-L. Lu, P.-F. Wang, S.-J. Ding, and D. W. Zhang, IEEE Electron Device Lett. **32**, 794 (2011).
[24] W.-Y. Chang, K.-J. Cheng, J.-M. Tsai, H.-J. Chen, F. Chen, M.-J. Tsai, and T.-B. Wu, Appl. Phys. Lett. **95**, 042104 (2009).
[25] D. Panda, A. Dhar, and S. K. Ray, IEEE Trans. Nanotechnol. **11**, 51 (2012).
[26] S. M. Sze, *Physics of Semiconductor Devices*, 2nd ed. (Wiley, New York, 1981).
[27] Y. C. Bae, A. R. Lee, J. B. Lee, J. H. Koo, K. C. Kwon, J. G. Park, H. S. Im, and J. P. Hong, Adv. Funct. Mater. **22**, 709 (2012).
[28] K. Jung, H. Seo, Y. Kim, H. Im, J. P. Hong, J.-W. Park, and J.-K. Lee, Appl. Phys. Lett. **90**, 052104 (2007).
[29] Y. Sato, K. Kinoshita, M. Aoki, Y. Sugiyama, Appl. Phys. Lett. **90**, 033503 (2007).
[30] J. Song, A. I. Inamdar, B. U. Jang, K. Jeon, Y. S. Kim, K. Jung, Y. Kim, H. Im, W. Jung, H. Kim, J. P. Hong, Appl. Phys. Express **3**, 091101 (2010).
[31] Y. Hosoi, Y. Tamai, T. Ohnishi, K. Ishihara, T. Shibuya, Y. Inoue, S. Yamazaki, T. Nakano, S. Ohnishi, N. Awaya, I. H. Inoue, H. Shima, H. Akinaga, H. Takagi, H. Akoh, and Y. Tokura, IEDM Tech. Dig. 793 (2006).
[32] D. C. Kim, S. Seo, S. E. Ahn, D.-S. Suh, M. J. Lee, B.-H. Park, I. K. Yoo, I. G. Braek, H.-J. Kim, E. K. Yim, J. E. Lee, S. O. Park, H. S. Kim, U.-I. Chung, J. T. Moon, and B. I. Ryu, Appl. Phys. Lett. **88**, 202102 (2006).
[33] I. Baek, M. Lee, S. Seo, M. Lee, D. Seo, D.-S. Suh, J. Park, S. Park, H. Kim, I. Yoo, U.-I. Chung, and J. Moon, IEDM Tech. Dig. 587 (2004).
[34] H. Jung, Y. Kim, K. Jung, H. Im, Y. A. Pashkin, O. Astafiev, Y. Nakamura, H. Lee, Y. Miyamoto, and J. S. Tsai, Phys. Rev. B **80**, 125413 (2009).
[35] J. H. Zheng, Q. Jiang, and J. S. Lian, Applied Surface Science **257**, 5083 (2011).
[36] H. Wang, S. Baek, J. Song, J. Lee, and S. Lim, Nanotechnology **19**, 7 (2008).